Available online at www.sciencedirect.com
ScienceDirect
Trans. Nonferrous Met. Soc. China 33(2023) 2599−2612
Transactions of Nonferrous Metals Society of China
www.tnmsc.cn

Construction of Al−Mg−Si−$Cu_{(p)}$ composite coating on aluminum alloy 1050 substrate

Hamed JAMSHIDI AVAL

Department of Materials Engineering, Babol Noshirvani University of Technology, Shariati Avenue, Babol 47148-71167, Iran

Received 16 January 2022; accepted 15 June 2022

Abstract: The AA6061 aluminum alloy matrix composite reinforced by copper particles was applied to the AA1050 aluminum substrate using a friction surfacing process. The effect of reinforcement content and pre-coating heat treatment condition of the consumable rod on the microstructure and mechanical properties was investigated. The results showed that coating with T6 treated consumable rod and increasing the mass fraction of copper powder resulted in higher temperature during friction surfacing. With increasing the mass fraction of copper powder, the average grain size of the coatings created with T6 and solid solutionized rods decreased. The average grain size of the coating in the samples created with the solid solutionized rod was 16% finer than that in the samples created with T6 rods. By increasing the mass fraction of copper to 20%, the wear resistance in coatings created with T6 and solid solutionized rods is increased by 28% and 24%, respectively, compared to that of the AA1050 substrate. Furthermore, by using a T6 rod and 20 wt.% copper, the shear strength, hardness, and wear resistance of the coating were 4%, 8%, and 5%, respectively, higher than those of the coating created with the solution-treated rod.

Key words: AA6061 matrix composite; friction surfacing; microstructure; pre-coating heat treatment

1 Introduction

Over the past decades, the metal-matrix composites (MMCs) have received more attention due to their various applications in industry, which are primarily due to the increased mechanical properties of the base metal after composite fabrication [1−4]. The application of high-strength composite coatings is one of the demands of the industry, which has been specially assessed by metallurgists for the past decades. Metal-matrix composite coatings are special surface coatings that can change some surface properties to a certain depth. Aluminum-matrix composites (AMCs) are among these composites, which are widely used in various industries. AA6061 aluminum alloy is an example of AMCs, which can increase the strength and surface properties due to its precipitation hardening ability. The presence of alloying elements such as magnesium and silicon in this group of aluminum alloys leads to the formation of intermetallic compounds, increasing the strength of the alloy [5,6].

In surface engineering, the production of composite coatings is divided into two main methods, solid and liquid states. In the liquid-state methods, the matrix melts; however, composite production is performed without melting the matrix in solid-state methods [7]. Laser cladding, vapor deposition, and centrifugal casting are examples of liquid-state methods with limitations, including hot cracking, porosity formation, and reinforcement agglomeration. Due to their unique characteristics, the solid-state methods are being replaced by conventional coating methods [8−10]. The method

Corresponding author: Hamed JAMSHIDI AVAL, Tel: +98-11-35501808, Fax: +98-11-35501800, E-mail: h.jamshidi@nit.ac.ir
DOI: 10.1016/S1003-6326(23)66284-3

of friction surfacing (FS) is among the solid-state methods with various advantages such as eliminating casting defects, controlling micro-structure, and improving strength.

Despite many advantages of the friction surfacing process in applying composite coatings, limited studies have been conducted in this field. GANDRA et al [11] investigated the wear properties of Al−SiC gradient composite coatings created by the friction surfacing process on AA2024 aluminum alloy substrates. The SiC particles with average sizes of 118.8, 37.4, and 12.3 μm were applied inside the AA6082 aluminum alloy consumable rod through drilling holes on it. It was reported that in different samples, when the number of holes is equal, finer SiC particles lead to a more uniform distribution of the reinforcing phase in the coating. It was observed that, unlike the coated sample without reinforcement, the presence of SiC particles in the coating prevents delamination and improves its wear resistance. NAKAMA et al [12] investigated the friction surfacing of the AA6061 aluminum alloy consumable rod on the AA6061 aluminum alloy substrate. They reported that coating at a pressure of 20 MPa was more efficient than coating at 25 MPa. Moreover, as the number of holes increases, the coating efficiency decreases. REDDY et al [13] investigated the formation of a metal-matrix composite coating on A356 aluminum alloy using the FS process. They reported that the coating showed excellent wear resistance, which was attributed to forming a metallurgical bond with the substrate. In addition, the coating presented a lower coefficient of friction and improved hardness compared to the A356 substrate. OLIVEIRA et al [14] investigated the FS of AA6351-T6 aluminum alloy reinforced by alumina particles on AA5052-H32 aluminum alloy substrate. The results showed that alumina particles increase the hardness of the coating. It was also observed that the grain size of the coating was 48% smaller than that of the base metal. SHARMA et al [15] investigated the surface modification of AA6061 aluminum alloy with FS of graphene and graphite containing consumable rods. The powder metallurgy has been used to prepare the consumable rod. It was observed that a significant improvement in the surface properties of aluminum alloy is achieved by applying graphene nanosheets to the coating. They showed that the friction coefficient of the applied coating using graphite particles with a size of 44 μm was reduced by 26.76% compared to the substrate.

The addition of copper in the aluminum matrix creates special properties such as increasing Young's modulus, toughness, and strength [16]. The commercially pure (CP) aluminum (such as AA1050 aluminum alloy) is widely used as a common metal in several applications, mainly due to its favorable corrosion resistance, formability, and high thermal conductivity. Nevertheless, the low strength and hardness of CP aluminum challenge its potential for industrial applications. The local treatment of CP aluminum can be alternatively used so that the strength and hardness of the alloy can be enhanced without sacrificing the favorable formability and corrosion resistance of the material. FS potentially seems to be a promising coating method as it encompasses a wide range of coatings with various properties. Accordingly, the present study aimed to improve the surface properties of AA1050 aluminum, including strength and hardness, by creating an AA6061 aluminum matrix composite coating. The aluminum matrix composite was obtained by drilling holes with different diameters on the cross-section of the consumable rod and filling them with copper powder. In this study, the effect of copper reinforcement mass fraction and pre-coating heat treatment of a consumable rod on the microstructure and mechanical properties of the AA6061-$Cu_{(p)}$ composite coating was investigated.

2 Experimental

In this study, the AA1050 aluminum sheet with a thickness of 4 mm was used as the substrate. Also, the AA6061 aluminum alloy rod with a diameter of 20 mm was used as the consumable rod. The AA1050 chemical composition was 0.07% Si, 0.28% Fe, 0.05% Cu, 0.02% Mn, 0.01% Mg, and balanced Al, and the AA6061 chemical composition is 0.62% Si, 0.57% Fe, 0.32% Cu, 0.11% Mn, 1.15% Mg, and balanced Al (all presented in mass fraction). The copper powder with a purity of 99% and a size of less than 100 μm was utilized as a reinforcing agent.

As shown in Fig. 1, two holes were drilled to apply copper powder to the cross-section of the consumable rod. Moreover, holes with a diameter of

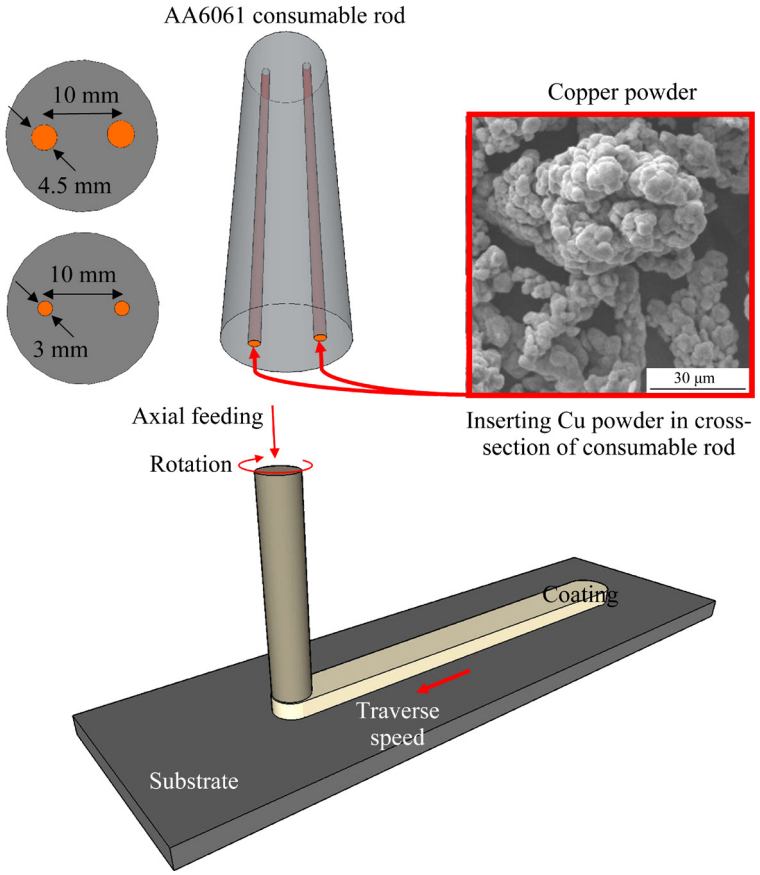

Fig. 1 Schematic illustration of consumable rod preparation and friction surfacing process

3 and 4.5 mm and a length of 60 mm were drilled to apply 10 and 20 wt.% of copper powder in the consumable rod. After drilling, the copper powder was applied to the holes. The coated samples were named according to Table 1. Friction surfacing was performed using a traverse speed of 125 mm/min, an axial feeding rate of 200 mm/min, and a rotational speed of 800 r/min.

Table 1 Information of coated samples

Sample	Copper content/wt.%	Consumable rod heat treatment condition
SS-0	0	Solid solutionized
SS-10	10	Solid solutionized
SS-20	20	Solid solutionized
T6-0	0	T6-treated
T6-10	10	T6-treated
T6-20	20	T6-treated

After coating, according to Fig. 2, different samples were extracted to evaluate the microstructure, mechanical properties, and wear properties of the applied coatings. Poulton's reagent

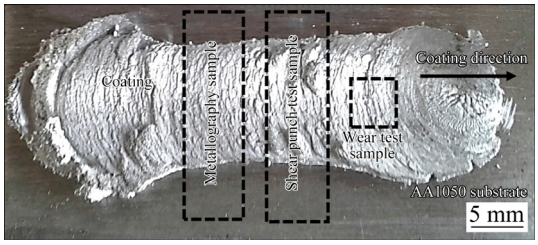

Fig. 2 Extraction position of microstructural, mechanical and tribological examination samples

(2 mL HF + 3 mL HCl + 20 mL HNO_3, 175 mL H_2O) was used to detect the microstructure. Optic microscopy and scanning electron microscopy were used to study the grain structure of the samples. Furthermore, a quantitative analysis of microstructural characteristics was performed using Clemex software. Grain size measurement was accomplished based on the linear intercept method and the ASTM E112 standard. X-ray diffraction patterns can be used for micro-strain (density of dislocations) stored in structures under severe plastic deformation.

The famous Scherer and Williamson−Hall methods are widely used for this purpose. Despite

the differences, both methods have been developed based on the relationship between grain size and micro-strain at full width at half maximum (FWHM). In this study, the Williamson−Hall method was used to estimate the density of stored dislocations, which is in the form of Eq. (1) [17]:

$$B\cos\theta=\frac{K\lambda}{D}+4\varepsilon\sin\theta \quad (1)$$

where B is the peak width at half-height, θ is diffraction angle, K is a constant of about 1, λ is X-ray wavelength, D is the average crystallite size, and ε is the average micro-strain of the lattice. Based on micro-strain and crystallite size, a method was introduced to estimate the density of dislocations in severely deformed structures (Eqs. (2)−(4)) [18]:

$$\rho=(\rho_D\rho_S)^{0.5} \quad (2)$$

$$\rho_D=3/D^2 \quad (3)$$

$$\rho_S=6\pi\varepsilon^2/b^2 \quad (4)$$

where ρ is the dislocation density, ρ_D is the contribution of the dislocation density of the crystallite size, ρ_S is the contribution of the displacement density of the micro-strain, and b is the amplitude of Burgers vector. A hardness test and a shear-punch test were used to evaluate the mechanical properties of the coating. The hardness test was performed based on the ASTM E92 standard with a load of 0.98 N and a dwell duration of 10 s. The shear-punch test was performed based on the method presented in Ref. [19] and using the SANTAM STM−250 instrument with a speed of 0.1 mm/min. The pin-on-disk (POD) test was used to assess the samples' wear qualities regarding ASTM G99 — 05. The POD experiment was performed on a counterface disc made of SAE-AISI 52100 steel with a hardness of 60 HRC at a linear speed of 50 cm/s.

3 Results and discussion

3.1 Macrostructure

The thickness and width of the coatings were measured after applying the coating. The results are shown in Fig. 3. As is evident, with increasing the mass fraction of copper powder, the coatings created with T6 and solid solutionized rods showed various thicknesses and widths. As shown in Fig. 4, the temperature at the tip of consumable rod in different samples was measured. As is observed, in both types of consumable rods, the temperature decreased during coating by increasing the mass fraction of copper powder. Moreover, the solid solutionized rod showed a lower tip temperature compared to the T6 rod. The temperature reduction could occur during the process by adding Cu powder to the consumable rod, as reported by other researchers [19], decreasing the effective cross-section of the consumable rod, changing the friction conditions, and absorbing part of the heat input by additives. The temperature difference between the solid solutionized and T6 rods is discussed as follows: the consumable rod tip temperatures were far higher than the temperature range required for the aging phenomenon in AA6061 alloy [20]. Therefore, during the FS process, the solid solutionized rod experienced the aging phenomenon, and its strength increased.

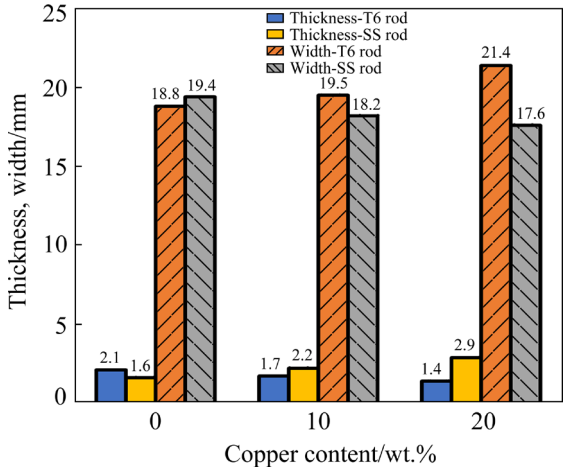

Fig. 3 Effect of copper content on thickness and width of coating

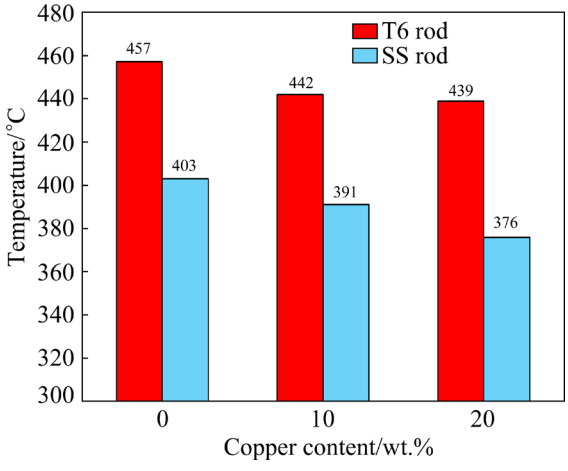

Fig. 4 Effect of copper content on temperature at tip of consumable rod

In addition, by increasing the strength of consumable rod, the plastic deformation of the rod decreased, resulting in decreasing the contact surface of the rod tip with the substrate. Under these conditions, the contribution of heat generated due to friction and plastic deformation was decreased, and the temperature during the process was reduced. However, in the T6 rod, the strength decreased due to the increase in temperature; therefore, the heat input increased due to plastic deformation and friction, resulting in more temperature during the process. As the temperature increased, the volume of the deposited material increased during the process; therefore, the geometric parameters of the coating (thickness and width) changed.

In the coating created with the solid solutionized rod, the width of the coating decreased by increasing the mass fraction of the copper powder. As mentioned earlier, as the mass fraction of copper powder increased, the tip temperature of the consumable rod decreased, resulting in decreasing the strength enhancement rate due to the aging phenomenon. As a result, the joint length between the deposited material and the substrate was reduced. On the other hand, reducing the strength of the consumable rod by increasing the mass fraction of the copper powder indicated the easier flow of the material at the rod tip, increasing the volume of the deposited material, thus increasing the thickness of the coating. Nevertheless, for the coating created with a T6 rod, increasing the mass fraction of copper powder resulted in decreasing the thickness of the coating and increasing the width of the coating. Therefore, less reduction in strength occurred in the consumable rod by increasing the mass fraction of copper powder. Under these conditions, the deformation capability of the consumable rod and the volume of the deposited material were reduced, leading to a reduction in the thickness of the coating. However, by reducing the tip temperature of the consumable rod, the difference between the flow stress of the consumable rod and the substrate increased, and more significant shear stress was created at the interface. The interaction of the substrate material and the deposited material occurred on a larger scale, and more strain was created at the interface, which provided a fresh substrate and created a wider effective joint.

3.2 Microstructure

Figure 5 shows the microstructure of different zones of coated samples with 10 wt.% copper with both solid solutionized and T6 consumable rods. In terms of grain size, the microstructure on various coating sections was not considerably different. Independent of the consumable rod's heat treatment circumstances, the distribution of reinforcing particles on both the advancing and retreating sides of all samples was more uniform than that of the center of the coating. Figure 6 shows the microstructure of the center zone of the coating in different samples. Also, the average grain size of different coatings is shown in Fig. 7. In all coatings, the microstructure included equiaxed, fine grains due to dynamic recrystallization during the coating process. As is evident, the average grain size of the coating in both coatings created with T6 and solid solutionized rods decreased by increasing the mass fraction of the copper powder. It should also be noted that the average grain size of the coating in the samples created with the solid solutionized rod was smaller than that of the samples created with T6 rod. In general, two factors of temperature and plastic strain were effective in forming recrystallized grains [21,22]. These two factors inversely affected the grain size; therefore, the recrystallized grain size decreased by decreasing temperature and increasing plastic strain. Due to the higher temperature and lower strength of the T6 rods during the coating process, the plastic strain increased during the coating. In this case, it can be said that the effect of temperature was predominant and increased the grain size of the coating. However, the two factors of temperature and plastic strain decreased the grain size of the recrystallized grain during coating with the solid solutionized rod. Due to lower plastic strain and temperature in the coating created with the solid solutionized rod, the effect of temperature was predominant, leading to smaller grain size. On the other hand, reducing the grain size of the coating by increasing the amount of copper indicated the decrease in temperature during the coating process and the presence of copper-rich particles that can act as nucleation sites of recrystallized grains through the particle stimulated nucleation (PSN) mechanism could be effective in reducing the grain size of the coating.

The microstructure of the interface and the upper zone of the coating in different samples is

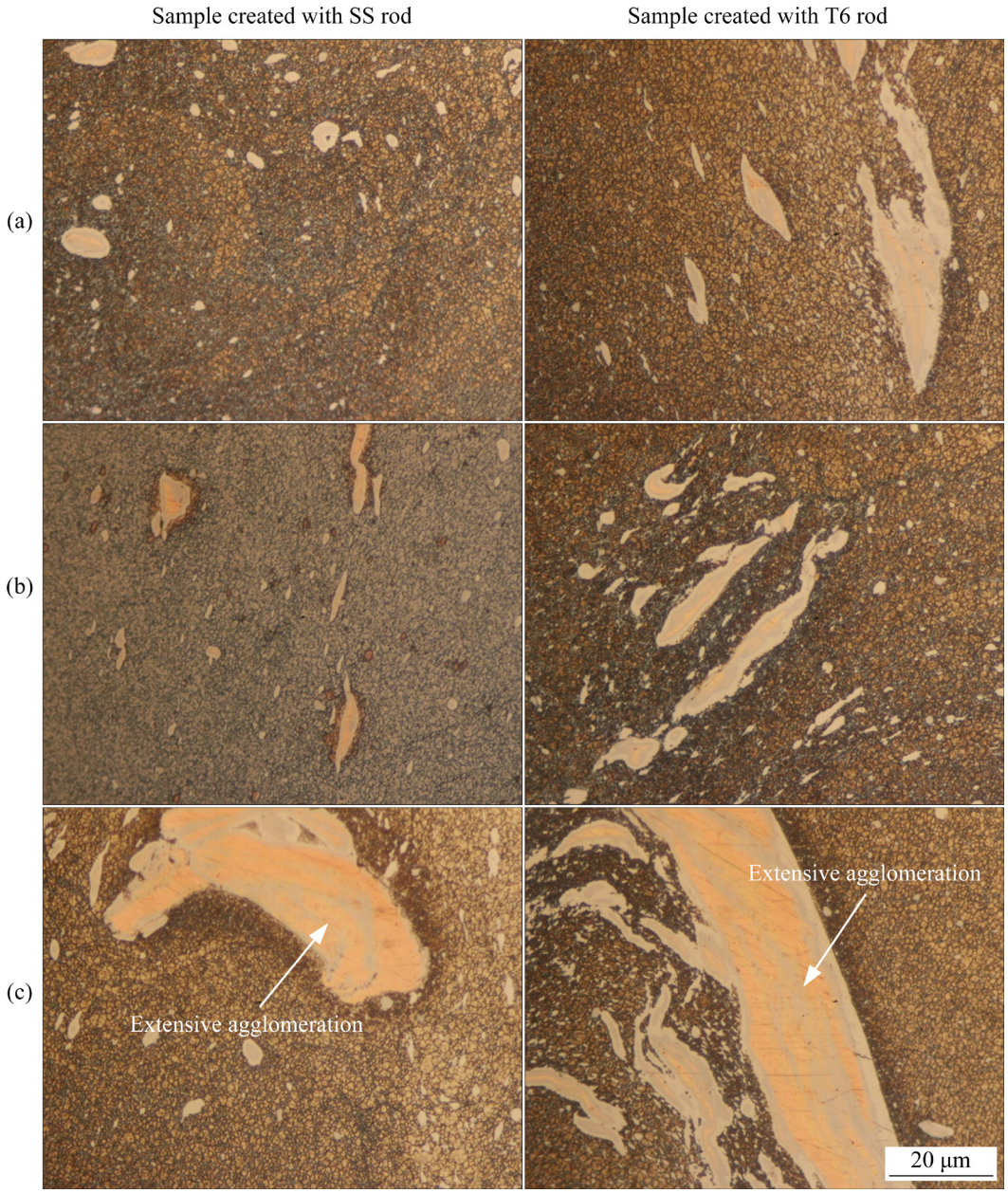

Fig. 5 Microstructure in different zones of coated samples with 10 wt.% copper: (a) Advancing side; (b) Retreating side; (c) Center zone

shown in Figs. 8 and 9, respectively. According to the EDS results (Fig. 10 and Table 2) and compared with previously reported results for AA6061 aluminum alloy [23−26], Mg_2Si, Si-rich, and Fe-rich precipitates and secondary phase particles were formed in the microstructure of all coatings. Cu-rich compounds were also formed in samples containing copper powder, as shown in Figs. 8 and 9. According to different sources [27,28], the average temperatures of formation and dissolution of the Mg_2Si precipitates are 332 and 435 °C, respectively. According to the temperature measurement during the coating process, the maximum temperature of coatings was higher than the dissolution temperature of Mg_2Si precipitates. Therefore, in all coatings, the complete and partial dissolution of Mg_2Si precipitates occurred in proportion to the strain conditions and temperature during the process.

According to SEM images of the samples coated with T6 rod, the size of Mg_2Si precipitates increased by reducing the heat input. In the coated sample without copper, the initial Mg_2Si precipitates in the coated sample were dissolved under the influence of temperature during coating, and the re-precipitation occurred during cooling.

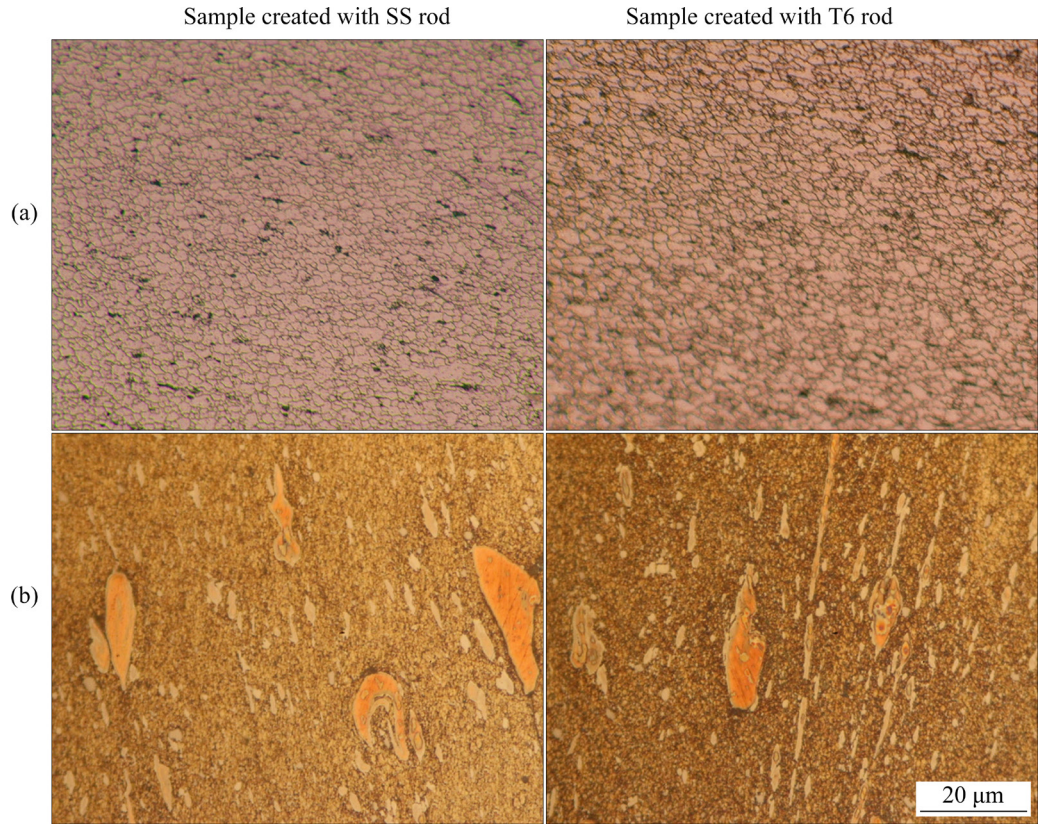

Fig. 6 Microstructure in center zones of coating: (a) Sample without reinforcement; (b) Sample with 20 wt.% copper

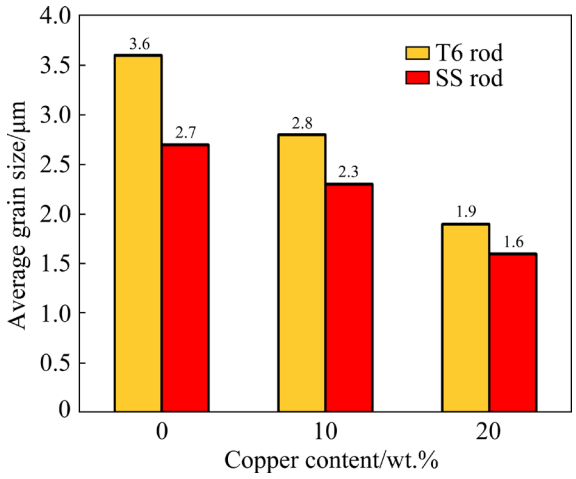

Fig. 7 Effect of copper content on coating grain size

However, in the copper-containing sample, due to the lower temperature during the coating, there was not enough opportunity for the complete dissolution of the initial precipitates, predominating the growth of precipitates. In samples coated with solutionized rods, the size of Mg_2Si precipitates increased by decreasing the heat input. Moreover, the size of Mg_2Si precipitates was more significant in the sample coated with solid solutionized rods. As the copper mass fraction increased, the size of Mg_2Si precipitates in the sample coated with the solid solutionized rod changed from 0.4 to 0.9 μm; however, the size of the precipitates changed from 0.3 to 0.7 μm in the sample coated with the T6 rod. Due to the presence of precipitation conditions in the solid solutionized rod, precipitation occurred, followed by growth of precipitates. In this case, there was less opportunity for re-precipitation. However, more opportunities were provided for the re-precipitation of new precipitates in the sample coated with the T6 rod due to the existence of Mg_2Si precipitates in the rod and the occurrence of dissolution and the growth of precipitates during the process. A comparison of copper particles in coated samples showed that regardless of the heat treatment conditions of the consumable rods, the thickness of the reaction layer and the number of copper particles were reduced at the interface with increasing the copper mass fraction. On the other hand, in the samples coated with T6 rod, the number of particles that reacted entirely with the aluminum matrix increased due to more uniform distribution and smaller size of Cu-rich particles. According to the EDS analysis and as shown Figs. 8 and 9, the reaction layers were $CuAl_2$ and CuAl.

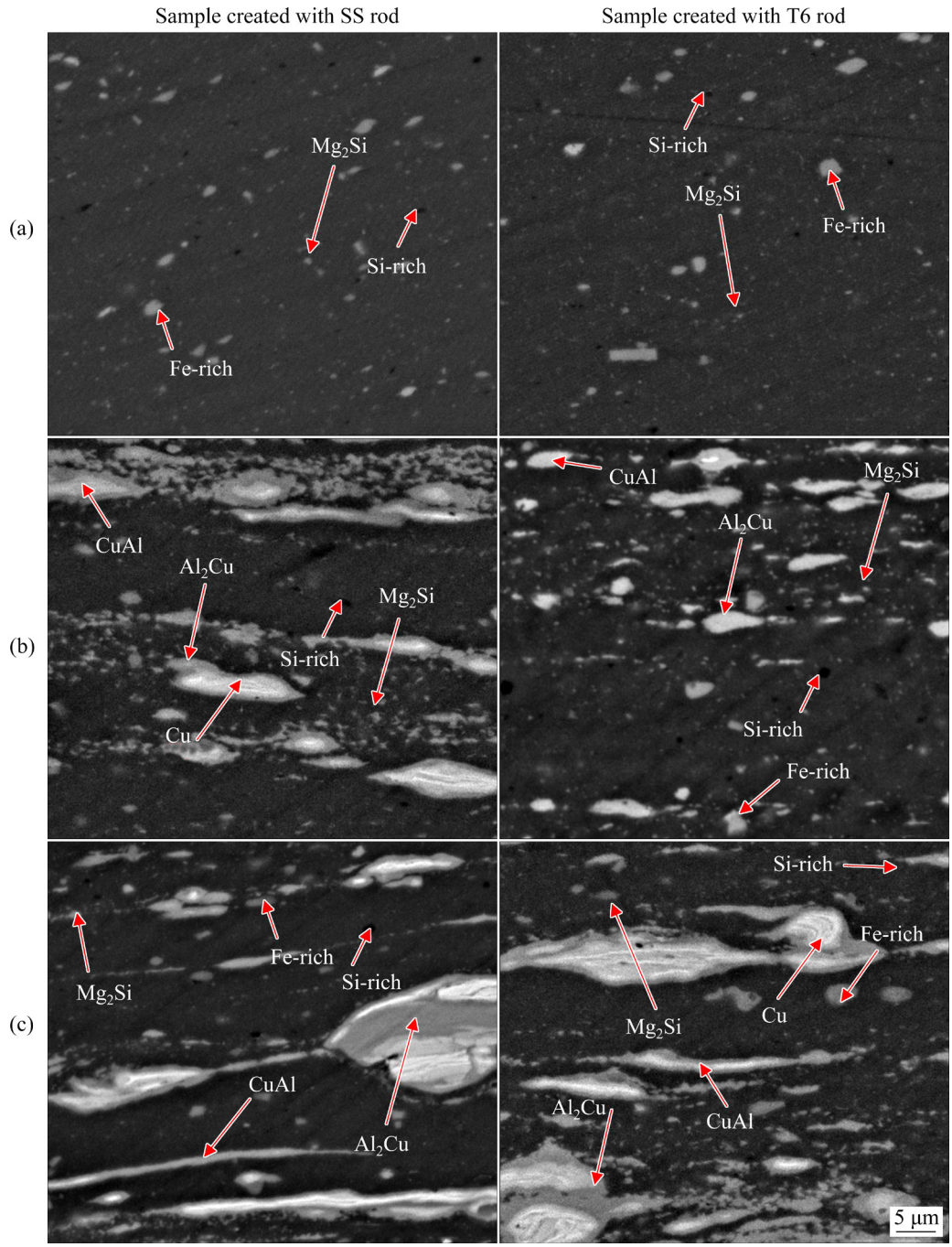

Fig. 8 SEM images of precipitates and second-phase particles at interface of coating with different contents of copper: (a) 0 wt.%; (b) 10 wt.%; (c) 20 wt.%

3.3 Mechanical properties

The hardness variations in the direction perpendicular to the interface of the coating/substrate are shown in Fig. 11. For all samples, the hardness of the coating created with the T6 rod was higher than that of the coating created with the solid solutionized rod. The hardness perturbation was observed in all coatings due to the collision of hardness indenter to the zone of accumulated copper particles. However, the hardness perturbation in other zones of the coating was negligible. It should be noted that these perturbations increased by increasing the amount of Cu-rich particles due to their non-uniform distribution. Hardness changes also indicated a higher hardness in the coating fabricated by the T6 rod. The average hardness, shear strength, and wear resistance test results of the coatings are shown in Fig. 12. As is observed, the hardness and shear strength increased with increasing the mass fraction of the copper powder.

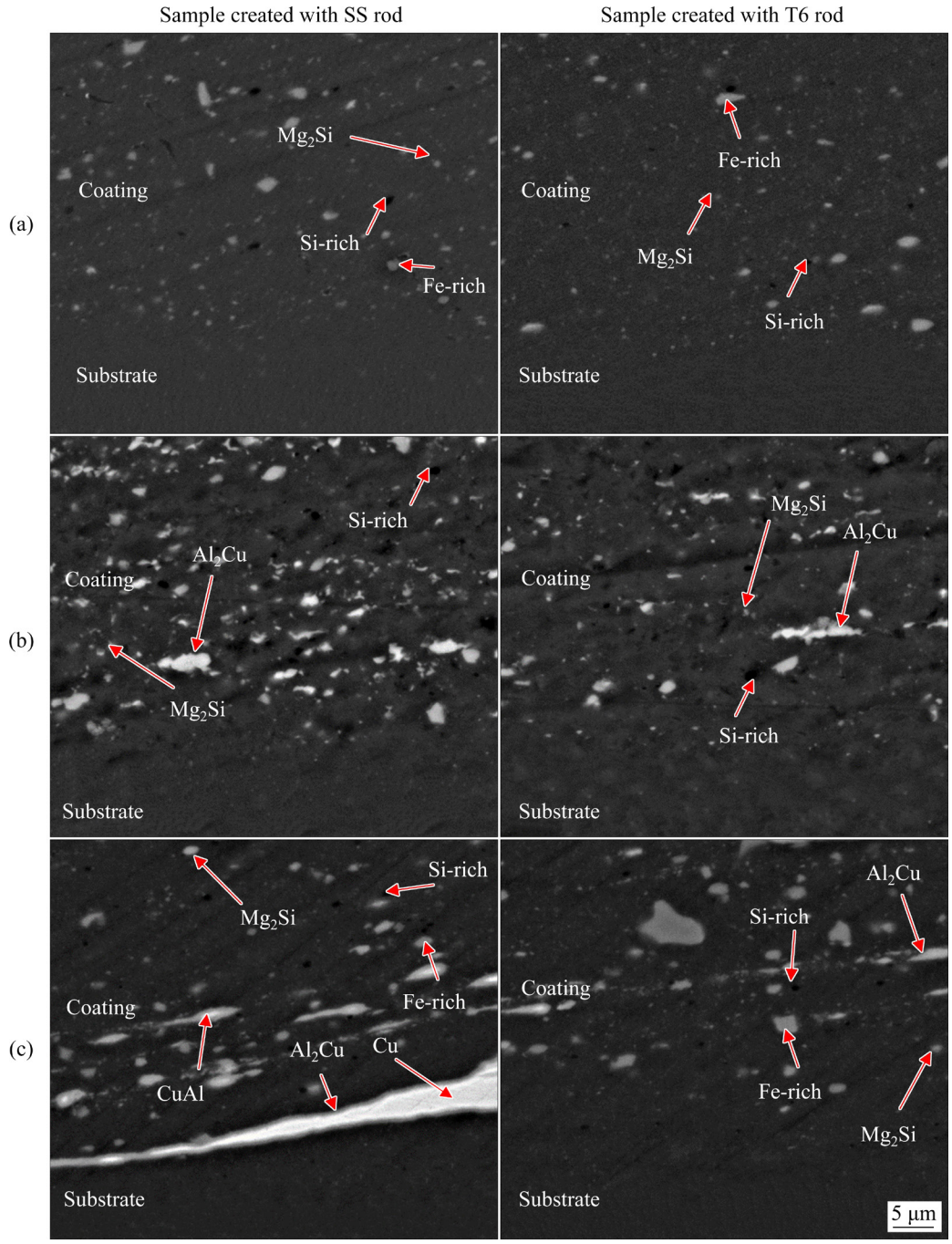

Fig. 9 SEM images of precipitates and second-phase particles in upper zone of coating with different contents of copper: (a) 0 wt.%; (b) 10 wt.%; (c) 20 wt.%

In all coatings, the hardness, shear strength, and wear resistance of the coating created with the solid solutionized rod was less than that created with the T6 rod. According to Ref. [29], wear rate and hardness were inversely proportional. According to the results of the microstructural part, the grain size of the coating decreased with increasing the reinforcing particles. The grain size reduction of the coating could act as an influential factor in increasing the strength and hardness of the coating. On the other hand, reducing the temperature during the process by increasing the mass fraction of copper powder could help increase the hardness and strength due to the formation of finer precipitates. The modulus strengthening mechanism was also effective in strengthening due to the presence of reinforcing particles. Although the distribution of particles was non-uniform by increasing the mass

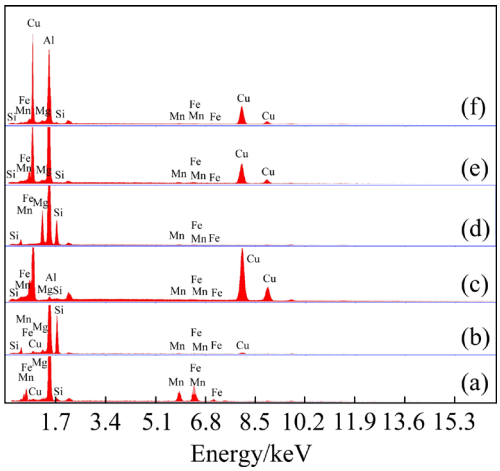

Fig. 10 EDS analysis results of precipitates and secondary phase particles: (a) Fe-rich; (b) Si-rich; (c) Cu-rich; (d) Mg_2Si; (e) $CuAl_2$; (f) CuAl

Table 2 EDS analysis results of Fe-rich (Spot I), Si-rich (Spot II), Cu-rich (Spot III), Mg_2Si (Spot IV), $CuAl_2$ (Spot V), and CuAl (Spot VI) (at.%)

Spot No.	Al	Mg	Si	Cu	Fe	Mn
I	85.54	0.05	1.01	0.08	10.11	3.21
II	84.28	1.2	14.11	0.05	0.11	0.25
III	2.11	0.58	0.09	95.93	0.51	0.78
IV	51.68	30.89	16.45	0.32	0.21	0.45
V	68.54	0.89	0.36	28.45	0.85	0.91
VI	54.95	0.75	0.62	42.11	0.71	0.86

fraction of copper powder, this non-uniform distribution affected the hardness distribution and standard deviation of shear strength. Nevertheless, eventually, the strength and hardness increased by increasing the mass fraction of copper powder. As

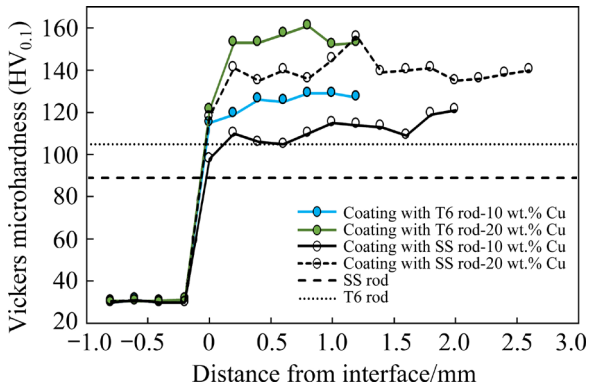

Fig. 11 Hardness profile perpendicular to coating/substrate interface of coated samples

can be seen, all coatings exhibit a lower wear rate and friction coefficient than consumable rods and substrate. Additionally, when coatings created with the solid solutionized consumable rod were compared to the substrate, wear resistance was increased by 16%, 20%, and 24% at copper contents of 0, 10, and 20 wt.%, respectively. According to Fig. 12(b), the wear resistance of coatings created with the T6 consumable rod was increased by 19%, 22%, and 28% relative to the substrate at copper contents of 0, 10, and 20 wt.%, respectively. As can be seen, the wear resistance and hardness of coatings are inversely proportional, i.e., increasing the hardness of the coating increases the wear resistance. Other studies have reported similar findings regarding the relationship between hardness and wear resistance [16,29]. In Table 3, the hardness and wear rate results in current study are compared to similar studies that have applied aluminum matrix composite coatings to aluminum substrates. The results indicate that when the copper

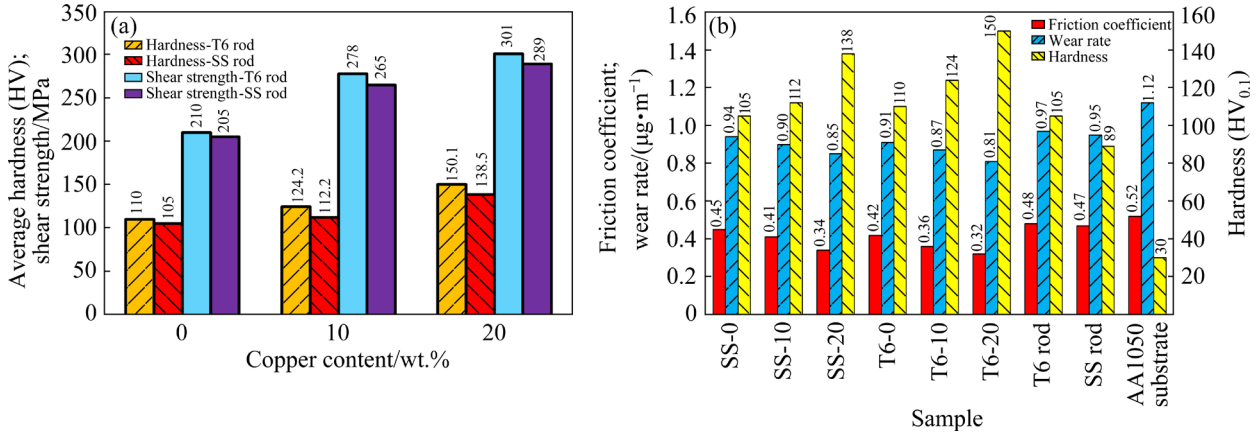

Fig. 12 Hardness and shear strength of coated samples (a) and wear test results of different samples (b)

powder is used as the reinforcement, the hardness and wear resistance significantly increase compared to the substrate.

The density of dislocations calculated by the X-ray diffraction pattern of different samples is presented in Table 4. As is evident, the density of dislocations after FS was significantly increased. Therefore, for the coating fabricated by the T6 rod, the density of dislocations for the reinforcement-free coating reached 11.43×10^{14} m^{-2}, indicating an increase of about 13% compared to the consumable rod. The increase in the density of dislocations was due to the entrapment of existing dislocations and the production of new dislocations [21]. Due to severe plastic deformation, various sources of dislocation production, such as Frank-Reid, were activated [30]. During deformation, the dislocations (with amplitude of Burger vector b) traveled the mean distance L, and the density of the dislocations was related to the real strain (ε) by Eq. (5) [21]:

$$\varepsilon=\rho bL \tag{5}$$

The distance L was generally considered the grain size or the distance between the reinforcing particles. According to Table 4, the presence of reinforcing particles in the composite sample increased the density of dislocations compared to the reinforcement-free sample. Therefore, the density of dislocations was increased from 12.11×10^{14} to 15.62×10^{14} m^{-2} by adding 20 wt.% of reinforcement to the solid solutionized rod. In general, increasing the density of dislocations during deformation and their interaction with each other is the main cause of strain hardening behavior in metals. After severe plastic deformation, the density of dislocations increased significantly. These dislocations were accumulated at the grain boundaries, forming non-equilibrium boundaries. These unbalanced grain boundaries could absorb dislocations within the grains, which reduced their accumulation and interaction within the grains. Therefore, the occurrence of recovery due to the absorption of dislocations by non-equilibrium boundaries reduced the strain hardenability of the samples. Also, in conditions where many dislocations were absorbed by these non-equilibrium boundaries, the slip conditions of grain boundaries were provided, which was another reason for reducing the strain hardening phenomenon in severely deformed samples.

The strengthening mechanisms in the coated samples were investigated to study the mechanical properties in detail. The effective reinforcement mechanisms for non-reinforcing aluminum coatings included fine forming of grain and precipitates and strain hardening due to severe plastic deformation. For the composite coatings, the direct effects of reinforcing particles on the strength and increasing the density of dislocations due to the difference between the thermal expansion coefficients of the matrix and the reinforcement were also investigated. The effect of the grain size on the strength enhancement was explained by the famous Hall−Patch relationship. The contribution of the strengthening mechanism due to the production of dislocations during the severe plastic deformation (SPD) in increasing the strength (σ_{Dis}) of the composite was given by Eq. (6) [31]:

$$\Delta\sigma_{Dis}=M\alpha Gb\rho^{0.5} \tag{6}$$

where M is the Taylor coefficient (3.06 for aluminum [32]), α is a constant equal to 0.24 [33], G is the shear modulus (26 GPa), and b is equal to 0.286 nm. Also, the following equation showed the effect of the strengthening mechanism due to the production of dislocations caused by the difference between the thermal expansion coefficient of the particles and the matrix ($\Delta\sigma_{CTE}$) [34]:

Table 3 Comparison of hardness and wear rate of present study with similar studies

Substrate	Coating		Property change comparing to substrate/%		Source
	Consumable rod	Reinforcement	Hardness improvement	Wear rate reduction	
A356	AA2024	SiC	282	97	[13]
AA6061	AA6061	Al_2O_3	86	23	[12]
AA2024	AA6082	SiC	30	−80	[11]
AA6061	Pure aluminum	Graphene	100	−	[15]
AA1050	AA6061	Cu	903	21	Present work

Table 4 Calculated dislocation density for different samples

Sample No.	Dislocation density/10^{14} m^{-2}
SS-0	12.11
SS-10	13.45
SS-20	15.62
T6-0	11.43
T6-10	12.98
T6-20	14.32
SS rod	7.14
T6 rod	10.12

$$\Delta\sigma_{\mathrm{CTE}}=\alpha Gb\left(\frac{12\Delta T\Delta C V_{\mathrm{P}}}{b\left(1-V_{\mathrm{P}}\right)d_{\mathrm{P}}}\right)^{0.5} \tag{7}$$

where ΔT is the temperature difference between the process and the test, ΔC is the difference between the thermal expansion coefficients, V_{P} is the volume fraction of reinforcing particles, and d_{P} is the size of precipitates/secondary phase particles. The effect of the direct strengthening mechanism due to the presence of reinforcing particles on increasing strength ($\Delta\sigma_{\mathrm{Load}}$) was investigated by Eq. (8) [35]

$$\Delta\sigma_{\mathrm{Load}}=0.5V_{\mathrm{P}}\sigma_{\mathrm{m}} \tag{8}$$

where σ_{m} is the yield strength of the matrix. The amount of strength enhancement caused by different mechanisms for the coatings without reinforcement and composite samples is presented in Table 5. On the other hand, the proportion of each reinforcement mechanism in increasing the strength of different samples is shown in Fig. 13. As is evident, the direct strengthening due to reinforcing particles, which did not play a role in strengthening the coating without reinforcement, was the most effective mechanism in the strengthening. Also, the strengthening by grain boundary was the second, and the strengthening mechanism due to the increase in the density of dislocations was the least effective mechanism in increasing the strength of the coatings.

The strengthening mechanisms in composites were divided into two categories: direct and indirect [36]. Direct strengthening occurred as a result of the load transfer mechanism from the matrix to the reinforcing particles. However, indirect strengthening arose from microstructural changes due to the presence of reinforcing particles in the composite matrix. The strengthening during SPD and grain refinement, both exacerbated by the presence of reinforcing particles, were examples of indirect strengthening. The strain hardening strengthening mechanism was affected by the presence of reinforcing particles. Therefore, the role of reinforcing particles in increasing the strength of the composite should not be limited to direct strengthening, and its positive effect on other strengthening mechanisms should also be considered.

Table 5 Strength enhancement caused by different mechanisms for coatings without reinforcement and composite samples

Sample No.	Strength increment by different mechanisms/MPa		
	Production of dislocations during FS	Grain refinement	Strengthening by reinforcement
SS-0	123.1	56.3	0
SS-10	151.2	69.4	77.4
SS-20	171.4	78.3	91.3
T6-0	111.2	51.2	0
T6-10	143.5	71.23	70.3
T6-20	161.7	79.31	80.0

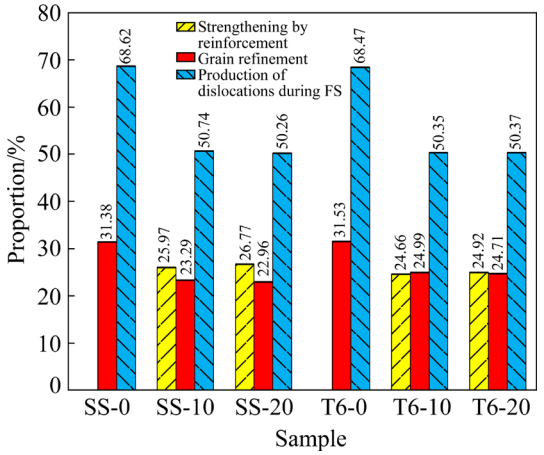

Fig. 13 Contribution of strengthening mechanism to predicted yield strength of different samples

4 Conclusions

(1) In friction surface-treated AA6061-$Cu_{(p)}$ composite coatings fabricated with both types of consumable rods (T6 and solid solutionized), the temperature decreased during coating by increasing the mass fraction of copper powder. Also, the temperature during coating with the solid solutionized rod was much lower than that

fabricated by the T6 rod.

(2) In the coating created with the solid solutionized rod, the width of the coating decreased by increasing the mass fraction of copper powder. However, in coating created with the T6 rod, with increasing the mass fraction of copper powder, the thickness and width of the coating decreased and increased, respectively.

(3) The average grain size of the coating in the samples created with the solid solutionized rod was finer than that of the samples coated with the T6 rods. The copper-rich particles in both coatings acted as nucleation sites of recrystallized grains through the PSN mechanism.

(4) In the samples coated with the T6 rod, the number of particles that reacted with the aluminum matrix increased due to more uniform distribution and smaller size of copper-rich particles.

(5) In the coatings created with the solid solutionized rod, by increasing the copper mass fraction from 0 to 20%, the coating's hardness and shear strength increased from HV 105 to HV 138.5 and 205 to 289 MPa, respectively, compared to the AA1050 substrate. Moreover, in the coatings created with the T6 rod, by increasing the copper mass fraction from 0 to 20%, the coating's hardness and shear strength increased from HV 110 to HV 150.1 and 210 to 301 MPa, respectively, compared to the substrate.

(6) The direct strengthening due to reinforcing particles played the most effective role in the strengthening. The strengthening by grain boundary was the second, and the strengthening mechanism due to the increase in the density of dislocations was the least effective mechanism in increasing the strength of the coatings.

References

[1] UYYURU R K, SURAPPA M K, BRUSETHAUG S. Tribological behavior of Al−Si−SiC_p composites/automobile brake pad system under dry sliding conditions [J]. Tribology International, 2007, 40(2): 365−373.

[2] NIE Q Q, CHEN G H, WANG B, YANG L, TANG W M. Process optimization, microstructures and mechanical/ thermal properties of Cu/Invar bi-metal matrix composites fabricated by spark plasma sintering [J]. Transactions of Nonferrous Metals Society of China, 2021, 31(10): 3050−3062.

[3] VICTOR CHRISTY J, ISMAIL MOURAD A H, SHERIF M M, SHIVAMURTHY B. Review of recent trends in friction stir welding process of aluminum alloys and aluminum metal matrix composites [J]. Transactions of Nonferrous Metals Society of China, 2021, 31(11): 3281−3309.

[4] GUAN Z P, LI M Y, XIA K X, LI Z G, GAO D, ZHAO P, MA P K, SONG J W. Microstructure, mechanical properties and wear resistance of SiC_p/AZ91 composite prepared by vacuum pressure infiltration [J]. Transactions of Nonferrous Metals Society of China, 2022, 32(1): 104−121.

[5] HOLLINGSWORTH E, HUNSICKER H. Corrosion of aluminum and aluminum alloys [M]. New York: ASM International, 1987: 583−609.

[6] WANG Q T, WANG X N, CHEN X M, HUAN P C, DONG Q P, ZHANG Q Y, NAGAUMI H. Interactive effects of porosity and microstructure on strength of 6063 aluminum alloy CMT MIX + Synchropulse welded joint [J]. Transactions of Nonferrous Metals Society of China, 2022, 32(3): 801−811.

[7] ESTHER I, DINAHARAN I, MURUGAN N. Microstructure and wear characterization of AA2124/4wt.%B_4C nano-composite coating on Ti−6Al−4V alloy using friction surfacing [J]. Transactions of Nonferrous Metals Society of China, 2019, 29(6): 1263−1274.

[8] FU Y, ZHANG Y B, JIE J C, SVYNARENKO K, LIANG C H, LI T J. Interfacial phase formation of Al−Cu bimetal by solid-liquid casting method [J]. China Foundry, 2017, 14(3): 194−198.

[9] SUNIL B R. Developing surface metal matrix composites: A comparative survey [J]. International Journal of Advances in Materials Science and Engineering, 2015, 4(3): 9−16.

[10] UYYURU R K, SURAPPA M K, BRUSETHAUG S. Effect of reinforcement volume fraction and size distribution on the tribological behavior of Al-composite/brake pad tribo-couple [J]. Wear, 2006, 260(11/12): 1248−1255.

[11] GANDRA J, VIGARINHO P, PEREIRA D, MIRANDA R M, VELHINHO A, VILAÇA P. Wear characterization of functionally graded Al−SiC composite coatings produced by friction surfacing [J]. Materials & Design, 2013, 52: 373−383.

[12] NAKAMA D, KATOH K, TOKISUE H. Fabrication of 6061 aluminum alloy/$A1_2O_3$ particle composites by friction surfacing [J]. Journal of Japan Institute of Light Metals, 2008, 58(7): 299−304.

[13] REDDY G M, RAO K S, MOHANDAS T. Friction surfacing: Novel technique for metal matrix composite coating on aluminium–silicon alloy [J]. Surface Engineering, 2009, 25(1): 25−30.

[14] OLIVEIRA P H F, GALVIS J C, PAULA MARTINS J, CARVALHO A L M. Application of friction surfacing to the production of aluminum coatings reinforced with Al_2O_3 particles [J]. Materials Research, 2017, 20(Suppl 2): 603−620.

[15] SHARMA A, SAGAR S, MAHTO R P, SAHOO B, PAL S K, PAUL J. Surface modification of Al6061 by graphene impregnation through a powder metallurgy assisted friction surfacing [J]. Surface and Coatings Technology, 2018, 337: 12−23.

[16] RAHMATI Z, JAMSHIDI AVAL H, NOUROUZI S, JAMAATI R. Effect of copper reinforcement on the microstructure, macrotexture, and wear properties of a friction-surfaced Al−Cu−Mg coating [J]. Surface and

Coatings Technology, 2022, 438: 128380.
[17] WILLIAMSON G K, HALL W H. X-ray line broadening from filed aluminium and wolfram [J]. Acta Metallurgica, 1953, 1(1): 22−31.
[18] FARSHIDI M H, KAZEMINEZHAD M, MIYAMOTO H. Severe plastic deformation of 6061 aluminum alloy tube with pre and post heat treatments [J]. Materials Science and Engineering A, 2013, 563: 60−67.
[19] PIRHAYATI P, JAMSHIDI AVAL H. Microstructural characterization and mechanical properties of friction surfaced AA2024−Ag composites [J]. Transactions of Nonferrous Metals Society of China, 2020, 30(7): 1756−1770.
[20] SONG Y, BAKER T N. A calorimetric and metallographic study of precipitation process in AA6061 and its composites [J]. Materials Science and Engineering A, 1995, 201(1/2): 251−260.
[21] HUMPHREYS F J, HATHERLY M. Recrystallization and related annealing phenomena [M]. Amsterdam: Elsevier, 2012.
[22] HUANG K, LOGÉ R. A review of dynamic recrystallization phenomena in metallic materials [J]. Materials & Design, 2016, 111: 548−574.
[23] MARIOARA C D, ANDERSEN S J, STENE T N, HASTING H, WALMSLEY J, VAN HELVOORT A T J, HOLMESTAD R. The effect of Cu on precipitation in Al−Mg−Si alloys [J]. Philosophical Magazine, 2007, 87(23): 3385−3413.
[24] MATSUDA K, SAKAGUCHI Y, MIYATA Y, UETANI Y, SATO T, KAMIO A, IKENO S. Precipitation sequence of various kinds of metastable phases in Al−1.0mass% Mg_2Si−0.4mass%Si alloy [J]. Journal of Materials Science, 2000, 35(1): 179−189.
[25] RAVI C, WOLVERTON C. First-principles study of crystal structure and stability of Al−Mg−Si−(Cu) precipitates [J]. Acta Materialia, 2004, 52(14): 4213−4227.
[26] GHAFERI M, MIRNIA M J, ELYASI M, JAMSHIDI AVAL H. Evaluation of different heat treatment cycles on improving single point incremental forming of AA6061 aluminum alloy [J]. The International Journal of Advanced Manufacturing Technology, 2019, 105(1): 83−100.
[27] SUMMERS P, LATTIMER B, CASE S. Residual constitutive behavior of aluminum alloys after fire exposure [J]. Fire Safety Science, 2014, 11: 612−625.
[28] BIROL Y. The effect of sample preparation on the DSC analysis of 6061 alloy [J]. Journal of Materials Science, 2005, 40(24): 6357−6361.
[29] ARCHARD J F. Contact and rubbing of flat surfaces [J]. Journal of Applied Physics, 1953, 24(8): 981−988.
[30] BRATOV V, BORODIN E N. Comparison of dislocation density based approaches for prediction of defect structure evolution in aluminium and copper processed by ECAP [J]. Materials Science and Engineering A, 2015, 631: 10−17.
[31] BOWEN J R, PRANGNELL P B, JUUL JENSEN D, HANSEN N. Microstructural parameters and flow stress in Al−0.13%Mg deformed by ECAE processing [J]. Materials Science and Engineering A, 2004, 387: 235−239.
[32] YOO S J, HAN S H, KIM W J. Strength and strain hardening of aluminum matrix composites with randomly dispersed nanometer-length fragmented carbon nanotubes [J]. Scripta Materialia, 2013, 68(9): 711−714.
[33] HANSEN N. Hall−Petch relation and boundary strengthening [J]. Scripta Materialia, 2004, 51(8): 801−806.
[34] KIM W J, PARK I B, HAN S H. Formation of a nanocomposite-like microstructure in Mg−6Al−1Zn alloy [J]. Scripta Materialia, 2012, 66(8): 590−593.
[35] MILLER W, HUMPHREYS F. Strengthening mechanisms in particulate metal matrix composites [J]. Scripta Metallurgica et Materialia, 1991, 25(1): 33−38.
[36] WANG Z, PRASHANTH K G, SCUDINO S, CHAUBEY A K, SORDELET D, ZHANG W W, LI Y Y, ECKERT J. Tensile properties of Al matrix composites reinforced with in situ devitrified $Al_{84}Gd_6Ni_7Co_3$ glassy particles [J]. Journal of Alloys and Compounds, 2014, 586: 419−422.

1050 铝合金基板上 Al−Mg−Si−$Cu_{(p)}$复合涂层的构建

Hamed JAMSHIDI AVAL

Department of Materials Engineering, Babol Noshirvani University of Technology, Shariati Avenue, Babol 47148-71167, Iran

摘　要：利用摩擦堆焊工艺在 AA1050 铝合金基板上制备铜颗粒增强 AA6061 铝合金基复合材料涂层。研究耗材棒的增强相含量和预涂层热处理条件对涂层显微组织和力学性能的影响。结果表明，使用 T6 处理的耗材棒和增加铜含量使摩擦堆焊过程的温度升高。随着铜粉含量的增加，使用经 T6 处理和固溶态耗材棒制备的涂层的平均晶粒尺寸均减小，且与 T6 处理相比，用固溶态耗材棒制备的涂层的平均晶粒尺寸细 16%。当铜的质量分数增加至 20%时，使用 T6 处理耗材棒和固溶态耗材棒制备的涂层的耐磨性分别比 AA1050 基板提高了 28%和 24%。此外，使用 T6 处理和添加 20%铜(质量分数)的耗材棒制备的涂层的剪切强度、硬度和耐磨性分别比使用固溶态耗材棒制备的涂层提高了 4%、8%和 5%。

关键词：AA6061 基复合材料；摩擦堆焊；显微组织；预涂层热处理

(Edited by Wei-ping CHEN)